The Effect of the Oceanic Boundary Layer on the Mean Drift of Pack Ice: Application of a Simple Model

MILES G. MCPHEE

U. S. Army Cold Regions Research and Engineering Laboratory, Hanover, NH 03755

(Manuscript received 28 April 1978, in final form 15 August 1978)

ABSTRACT

Smoothed records of ice drift, surface wind and upper ocean currents at four manned stations of the 1975–76 AIDJEX experiment in the central Arctic have been analyzed to provide a statistical relationship between stress at the ice-ocean interface and ice-drift velocity during a 60-day period when the ice was too weak to support internal forces. Using interfacial stress calculated from a balance with air stress and Coriolis force on the ice column for times longer than the inertial period, logarithmic linear regression of the stress-velocity samples provided the relation $\tau = 0.010V^{1.78}$, where τ is the magnitude of interfacial stress and V the ice speed relative to the geostrophic current in the ocean. This result is statistically indistinguishable from predictions of a numerical model adapted from Businger and Arya (1974) with surface roughness $z_0 = 10$ cm. Essential features of the model are dynamic scaling by u_*, u_*^2 and u_*/f for velocity, kinematic stress and length, with exponential attenuation of a linear dimensionless eddy viscosity, *viz.*, $K_* = -k\xi e^{c_1\xi}$, where $\xi = fz/u_*$ and k is von Kármán's constant. Currents measured 2 m below the ice confirmed the shape of the τ vs V curve and provided an estimate of the angle between surface stress and velocity. The model was used to qualitatively estimate the effect of a pycnocline at 25 m on surface characteristics. The observed behavior when stratification at that level was most pronounced tended toward slightly higher drag at higher speeds, which is qualitatively consistent with the model results.

1. Introduction

Studies of upper ocean dynamics staged from drifting pack ice offer at least two advantages rarely encountered in experiments performed at sea. First, the ice provides a stable, slow-moving platform from which delicate and precise instruments can be deployed and recovered easily. Second, the surface velocity of the ocean, which is just the ice velocity, can be measured accurately with modern navigational techniques. The latter, while perhaps not so obvious, becomes particularly important during periods when the pack is too weak to support a significant internal stress gradient, for then one can measure or closely estimate two fundamental aspects of the oceanic boundary layer, namely, surface stress and velocity, without (figuratively) getting his feet wet.

In the AIDJEX (Arctic Ice Dynamics Joint Experiment) series of ice floe stations, there have been several experiments designed to describe and understand the structure of the planetary boundary layer (PBL) that develops beneath pack ice as surface winds drive it across the ocean. In the pilot study of March–April 1972 an extensive program was carried out in which mean flow, turbulent fluctuations and upper ocean density were measured continuously at many levels for several weeks (McPhee and Smith, 1976). One result from that study was that a conceptual framework developed mainly for describing the neutrally stable atmospheric PBL seemed appropriate for the under-ice boundary layer, and we were able to show that predictions of turbulent velocity structure from Deardorff's (1972) three-dimensional numerical integration and from a second-order closure technique applied by Wyngaard *et al.* (1974) were similar to what we measured. A third model, that of Businger and Arya (1974), which closes the momentum equations at first order, also did an adequate job of describing the main features observed, while retaining a simplicity lacking in the others. In each case, the link allowing comparison of oceanic measurements with atmospheric models is a similarity scaling of velocity, kinematic stress and depth by u_*, u_*^2 and u_*/f, where u_* is the surface-layer friction velocity (i.e., the square root of kinematic stress in the surface layer) and f is the Coriolis parameter.

A notable feature of the 1972 experiment was that the ice drift was quite straight during the storms from which most of our useful data came. This was fortunate in that it allowed the PBL to reach a reasonably steady state. However, the lack of inertial motion, which would have shown up as cycloidal loops in the camp trajectory, made extrapolation of our results to the open ocean question-

0022-3670/79/020388-13$07.25

able. There the surface is unconstrained, and from all indications, inertial currents are ubiquitous. Thus it is reasonable to ask how large-amplitude horizontal oscillation might modify the conceptual model that emerged from the 1972 measurements before suggesting it is generally appropriate.

The AIDJEX main experiment, which maintained a triangle of three manned drift stations in the central Arctic from April 1975 to May 1976 offered a chance to test the effects of inertial waves. Beginning in late July of 1975, ice drift at all the stations (including a fourth, central camp which was later abandoned) was characterized by energetic and persistent inertial motion. An immediate inference was that the ice had become too weak to quell the motion and, therefore, the momentum balance must be essentially local. This was confirmed by simulations of the inertial velocity waves using a simple balance of total net transport multiplied by f and the local wind stress (McPhee, 1978a). Subsequent work comparing observed and simulated drift from which inertial-period energy had been filtered (McPhee, 1977a) also indicated that during this period the ice was essentially free of internal forces.

Unfortunately, measurements of currents in the boundary layer during the main experiment were sparse by comparison with the earlier work, consisting mainly of Savonius-rotor current meters suspended 2 and 30 m below the ice. [A detailed description is given in McPhee (1978b).] Without direct observations it was impossible to say, for example, how turbulent energy profiles were affected by the rapid temporal changes. On the other hand, the 1975 measurements provided a much larger statistical sample of gross characteristics of the ice-ocean boundary layer than had been available before, e.g., over a 60-day period in which the ice was believed to be free of internal force, we had about 230 camp-days of ice velocity, surface wind and near-surface current measurements.

The intent of this paper is thus to complement the earlier work by comparing statistics of ice drift in summer with a specific steady-state PBL model (Businger and Arya, 1974) in hopes of better understanding what effect inertial motion might have on time-averaged mean properties of the boundary layer (for example, do the oscillations spread the momentum evenly throughout the mixed layer, thus breaking down the u_*, u_*/f scaling?).

In the next section, the model is presented along with sample calculations pertinent to the ice-ocean boundary layer. In Section 3, two methods for inferring the stress-surface velocity relationship from available AIDJEX data are discussed, and statistical properties of the data are compared with model predictions. Section 4 contains a brief discussion of what effect the quasi-permanent summer pycnocline might have on the system. In Section 5 the work is summarized and similarity constants appropriate for the ice-ocean boundary layer are presented.

A further goal of the paper is to demonstrate that work carried out in the comparatively benign experimental environment of a drifting ice floe may have wide applicability in understanding the general PBL problem.

2. The model

Following the notation of Businger and Arya (1974), we align the x axis with stress at the ice-ocean interface and nondimensionalize the steady, horizontally homogeneous momentum equation to obtain

$$v - v_g = -\frac{\partial T_x}{\partial \xi}, \tag{1}$$

$$u - u_g = \frac{\partial T_y}{\partial \xi}, \tag{2}$$

where

$$(u,v) = (\hat{u}/u_*, \hat{v}/u_*),$$

$$(u_g, v_g) = \frac{g}{f u_*}\left(-\frac{\partial \eta}{\partial y}, \frac{\partial \eta}{\partial x}\right),$$

$$(T_x, T_y) = \frac{\tau_x}{u_*^2}, \frac{\tau_y}{u_*^2},$$

$$\xi = fz/u_*.$$

Here $\hat{u}$, $\hat{v}$ are dimensional current components; g is the acceleration of gravity; η is the sea surface elevation; and τ_x, τ_y are horizontal components of kinematic turbulent stress. Boundary conditions are

$$(u,v) = (u_g, v_g) \quad \text{as} \quad \xi \to -\infty,$$

$$\left.\begin{aligned} T_x &= 1 \\ T_y &= 0 \end{aligned}\right\} \xi = \xi_0 = f z_0/u_*,$$

where z_0 is the surface roughness. Note that ξ_0 is the inverse of the surface Rossby number $\mathrm{Ro}_* = u_*/f z_0$.

In the usual manner, first-order closure is accomplished by expressing the stress in terms of an eddy viscosity times the vertical shear in the mean flow, i.e., in nondimensional representation,

$$(T_x, T_y) = K_*\left(\frac{\partial u}{\partial \xi}, \frac{\partial v}{\partial \xi}\right), \tag{3}$$

where $K_* = fK_m/u_*^2$ and K_m is the eddy momentum exchange coefficient. Businger and Arya (1974) use what is basically an intuitive argument to formulate their K_* distribution, which will be paraphrased at some length here in order to demonstrate its applicability to the oceanic problem.

Essentially, the eddy viscosity concept relates the

turbulent overturn of fluid parcels possessing differing amounts of momentum in a shear flow to a mixing length and a turbulent velocity. At some level near a flat surface it seems clear that the vertical dimension of an eddy carrying momentum from that level toward the surface must be of the same order as the distance to the surface and, in fact, a preponderance of evidence suggests that the relationship between mixing length and distance is approximately linear, with the proportionality given by von Kármán's constant ($k = 0.40$). Now in a rotating fluid, there is an additional constraint, namely, that as distance from the surface increases, there is some point where the mixing eddies reach a limiting maximum dimension—probably related to an instability in the governing physics (see, e.g., Stern, 1975, p. 117). Past this point, the turbulent energy and thus the scaling velocity fall off. Therefore, on heuristic grounds, we expect the eddy viscosity to increase linearly with distance near the surface, to reach a maximum at some level, and to fall off beyond that. Such behavior has been confirmed by numerical experiments with the three-dimensional Navier-Stokes equations (Deardorff, 1972) and by PBL spectra measurements (McPhee and Smith, 1976).

A simple analytic expression having these properties is given by

$$K_* = -k\xi \exp(c_1\xi), \quad \xi < 0.$$

As in Businger and Arya (1974), the constant c_1 is evaluated by examining the behavior of the equations near the surface, i.e., for $|\xi|$ small. In that case

$$K_* \approx -k\xi(1 + c_1\xi). \tag{4}$$

Empirically, it is known that u varies logarithmically in the surface layer (we are considering only the neutral case here) and thus

$$\frac{\partial u}{\partial \xi} \approx -\frac{1}{k\xi}. \tag{5}$$

Therefore

$$T_x = K_*(\partial u/\partial \xi) \approx 1 + c_1\xi$$

and from the momentum equation in the surface layer, we have

$$\begin{aligned} v_s - v_g &= -\partial T_x/\partial \xi \approx -c_1, \\ K_* &= -k\xi \exp[(v_g - v_s)\xi]. \end{aligned} \tag{6}$$

We can eliminate (u_g, v_g) by considering a reference frame advected by the geostrophic flow. This requires that absolute ice velocity data be adjusted by that amount for comparison, but this is not a severe limitation since geostrophic currents due to sea surface tilt in the central Arctic are typically less than 2 cm s^{-1}.

Eqs. (1) and (2) are differentiated, and (3) is substituted to obtain a pair of coupled, second-order equations,

$$\frac{\partial^2 T_x}{\partial \xi^2} = \frac{-T_y}{K_*}, \quad \frac{\partial^2 T_y}{\partial \xi^2} = \frac{T_x}{K_*},$$

which can be solved for an arbitrary K_* distribution using an implicit numerical scheme (e.g., see Timokhov *et al.*, 1976). Since at the outset v_s in (6) is unknown, a value is assumed and solutions are performed iteratively until the change in v_s from one solution to the next falls below a specified tolerance.

Fig. 1 shows a solution for $\mathrm{Ro}_* = 1000$. The hodograph showing a horizontal projection of the mean velocity spiral provides a graphical link to the atmospheric problem. Viewed this way, the ice velocity is clearly analogous to the negative of the geostrophic wind. An observer drifting with the ice sees a current structure similar to that of the atmosphere, with large shear near the surface and gradual turning with depth toward a "free stream" value. The angle of turning, β, between ice motion and stress direction is exactly analogous to the geostrophic departure angle (usually called α) in the atmosphere. Note that a current meter suspended from the ice at $0.02\ u_*/f$, for example, would measure a current in nearly the opposite direction as the surface stress, and would be analogous to an anemometer on a tower at the corresponding nondimensional height in the atmospheric PBL.

The nondimensional surface speed $[S = (u^2 + v^2)^{1/2}]$ is 13.66, which implies a "geostrophic" drag coefficient ($c_w = S^{-2}$) of 0.0054. This example was thus not chosen entirely at random since in simulations of summer ice drift (McPhee, 1977a) we obtained reasonable results using constant values of the boundary layer parameters: $c_w = 0.0055$ and $\beta = 23°$. A typical ice-water kinematic stress during summer is of order 1 $cm^2\ s^{-2}$; thus for $\mathrm{Ro}_* = 1000$, we might expect z_0 to be of order 10 cm and an approximate PBL scale depth, $0.5\ u_*/f$, to be 35 m.

The general form of the velocity and stress distribution in Fig. 1 is not overly sensitive to the shape of the K_* distribution as long as it is approximately linear near the surface. Fig. 2 shows a calculation using a simple linear increase of K_* with depth until it reaches a maximum value of 0.022 which it retains for greater depths. Note that surface velocity characteristics ($c_w = 0.0054$, $\beta = 23.1°$) are similar to the previous example provided Ro_* is 1310, corresponding to roughly a 30% decrease in z_0, other things being equal. The shapes of the velocity and stress profiles are not significantly different. The advantage of the Businger and Arya (1974) approach is that the iterative process of letting the lateral surface velocity seek its own value eliminates the need for arbitrarily specifying, for example, a maximum value for K_*.

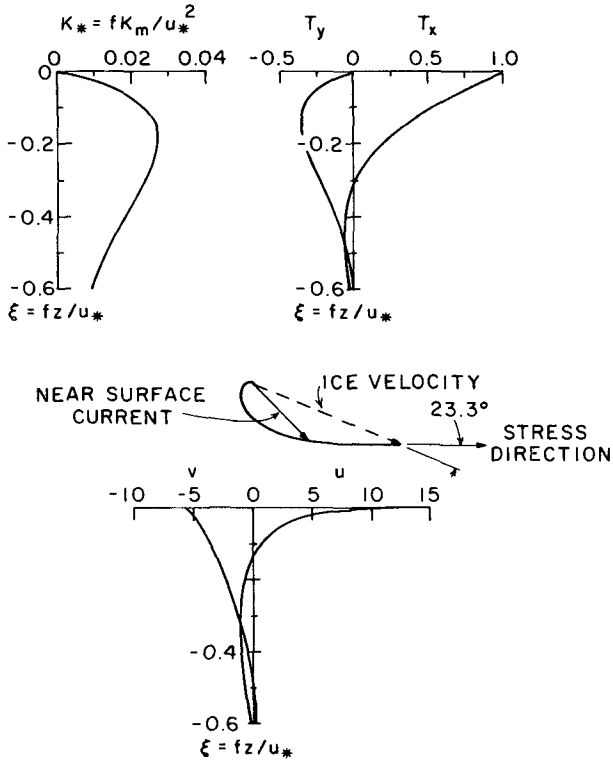

FIG. 1. Solutions of the PBL equations for $Ro_* = 1000$ showing profiles of dimensionless eddy viscosity, stress and velocity: $c_w = 0.0054$. The nondimensional depth of a point on the hodograph can be ascertained by dropping a vertical to the u profile.

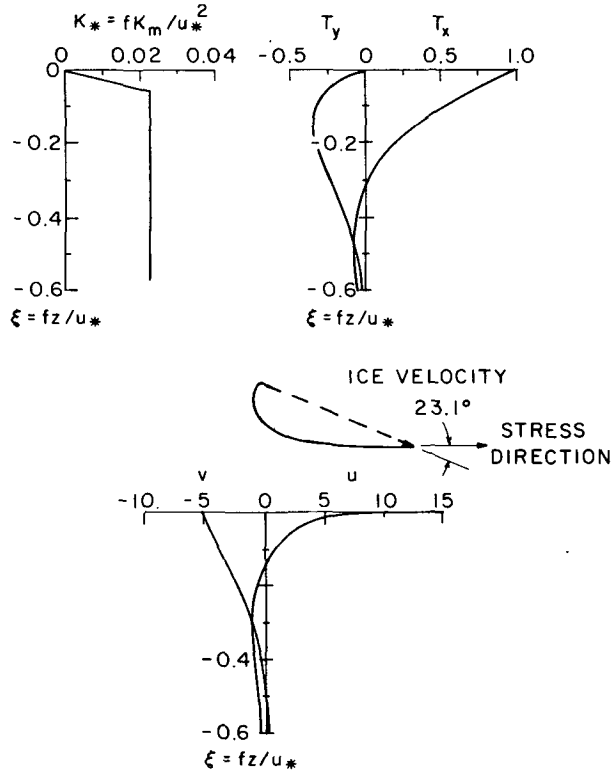

FIG. 2. As in Fig. 1 except $Ro_* = 1310$ and K_* distribution as shown. Maximum value of K_* is 0.022.

The behavior of solutions near the surface is highly dependent on the numerical value of Ro_*: for small $|\xi|$, integration of (5) yields

$$u_s - u(\xi) = k^{-1}(\ln|\xi| + \ln Ro_*).$$

Fig. 3 shows a PBL solution for $Ro_* = 10^5$. The difference in surface characteristics is due almost entirely to increase in shear of the u component for $|\xi|$ less than, say, 0.01. Clearly, z_0 is crucial if the main concern is surface velocity, as it is for predicting ice drift; but if the primary interest is in mean flow or turbulent energy levels at greater depths, the effect of changing z_0 is minimal as long as u_* and f remain unchanged. This is a fundamental point regarding extrapolation of these results to the open ocean. It would be fortuitous if the details of the free ocean surface were such as to give a surface velocity similar to that of the ice under similar stress conditions; however, barring some deep-penetrating surface phenomenon present in the open ocean (e.g., Langmuir cells), there is no reason to think the structure would be much different below a few meters depth.

For comparison with measured data, it is necessary to consider a range of values for Ro_* reflecting changes in u_* as the ice speed varies. Using several

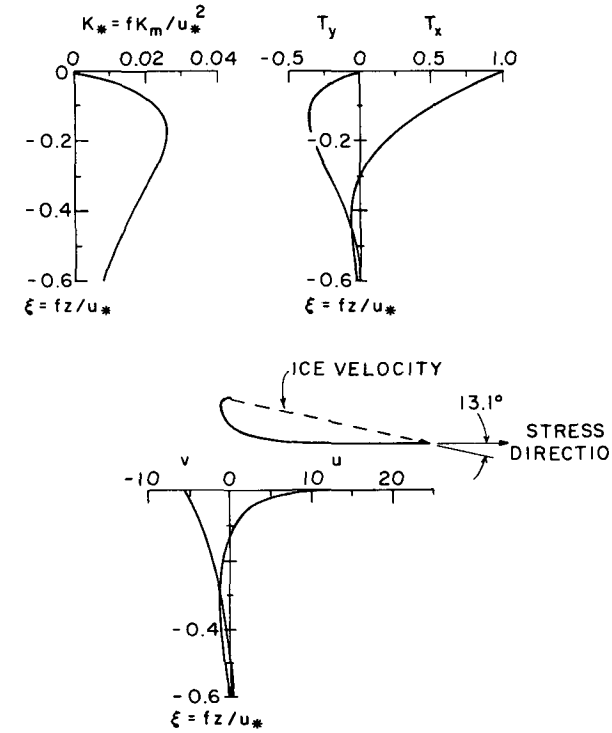

FIG. 3. As in Fig. 1 except $Ro_* = 10^5$, $c_w = 0.0016$.

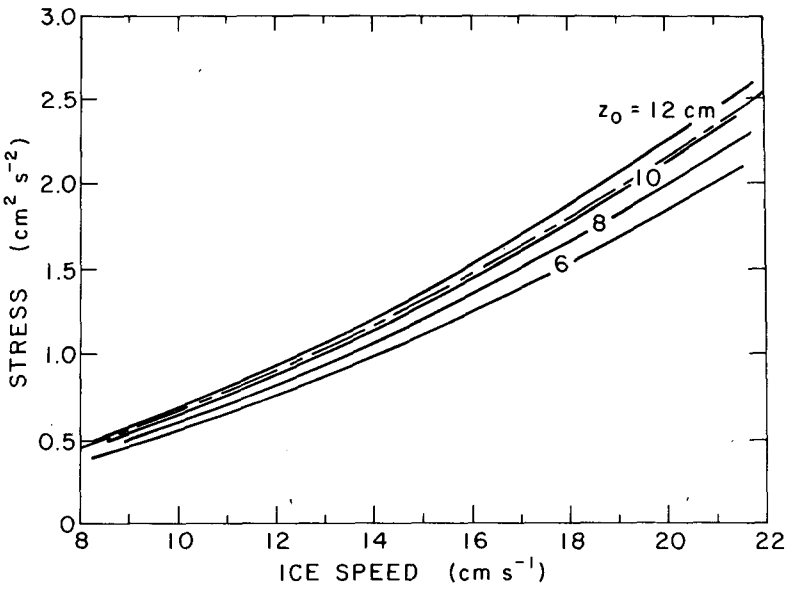

FIG. 4. Contours of kinematic surface stress versus ice speed for various values of surface roughness z_0. The broken curve is explained in Section 5.

plausible values for z_0, it is possible to construct curves of dimensional kinematic stress (u_*^2) versus ice speed by choosing samples of u_*, then solving the PBL equations with the appropriate Ro_* for each z_0 to determine the surface velocity. Results for z_0 ranging from 6 to 12 cm are shown in Fig. 4. Similarly, values for β can be calculated from the surface velocity as functions of ice speed and z_0. Finally, the current at a particular dimensional level (in our case, 2 m below the ice) relative to an observer drifting with the ice can be determined by finding the current at the proper nondimensional level in each model calculation and subtracting the surface velocity. The angle between this relative current and the negative ice velocity, which we shall call β_2, will approach β as the ice speed increases. Fig. 5 shows contours of β and β_2 for various values of z_0.

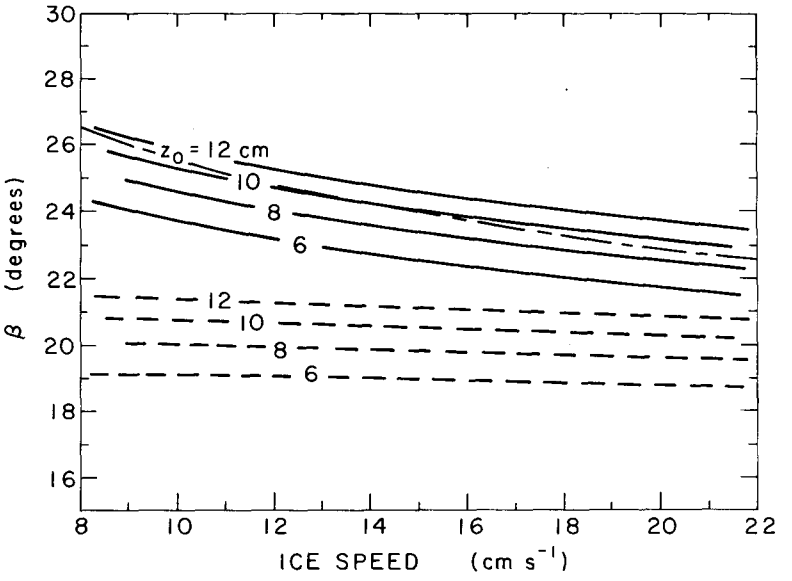

FIG. 5. Contours of β, the angle between ice drift and surface stress (solid lines) and β_2, the angle between negative ice velocity and current at 2 m relative to an observer drifting with the surface velocity. The broken β curve is explained in Section 5.

3. Observations

By assuming there are identifiable periods when pack ice is free of internal stress gradients, it is possible to compile a set of statistics relating stress at the ice–ocean interface to ice velocity relative to the undisturbed ocean. In an earlier work (McPhee, 1977a), we cited the presence of inertial oscillations, the relative uniformity of averaged wind-ice drift characteristics, and the success of simple ice drift simulations during the period 20 July 1975 to 18 September 1975 (days 201–261) as factors indicating the absence of internal ice force. Under these conditions, the *steady-state* momentum balance is quite simple, as diagrammed in Fig. 6.

The resultant sum of surface wind stress and Coriolis force on the moving ice column is stress acting on the ocean surface at an angle β counterclockwise from the drift direction. If we express vectors as complex numbers, with the relative velocity $\mathbf{V} = \mathbf{V}_I - \mathbf{V}_g$, where $\mathbf{V}_I$ is the absolute ice velocity and $\mathbf{V}_g$ is geostrophic flow in the mixed layer due to sea surface tilt, the momentum balance is

$$\rho_w \boldsymbol{\tau}_w = \rho_a c_{10} U_{10} \mathbf{U}_{10} - imf\mathbf{V}, \qquad (7)$$

where m is the ice mass per unit surface area, $\mathbf{U}_{10}$ is the wind at 10 m ($U_{10} = |\mathbf{U}_{10}|$), c_{10} is the 10 m drag coefficient, and ρ_a and ρ_w are air and water densities, respectively. Given measured values of $\mathbf{V}_I$ and $\mathbf{U}_{10}$ along with reasonable estimates for c_{10}, m and $\mathbf{V}_g$, $\boldsymbol{\tau}_w$ can be calculated for each sample.

In processing the AIDJEX data, records of ice velocity, 10 m winds and currents measured at 2 m with respect to the ice were smoothed with a cosine-bell convolution to eliminate energy at periods less than 12 h, which effectively filtered out most of the inertial period motion. The smoothed data were then sampled twice daily to construct a population of 480 samples each of $\mathbf{V}_I$, $\mathbf{U}_{10}$ and $\mathbf{U}_2$, the 2 m current *measured relative to the drifting ice*.

Next the ice velocity samples were corrected for the effects of sea surface tilt by subtracting $\mathbf{V}_g$. The objective here was to place the ice in a reference system in which it was at rest under conditions of no stress, a close approximation being a frame drifting with the mean geostrophic surface current. Unfortunately, our knowledge of the surface dynamic topography for the time in question is limited. Neither STD measurements nor deep current records were accurate enough (at least at the present stage of analysis) to shed much light here (McPhee, 1978b); thus we utilized a slightly modified version of dynamic topography compiled from historical data by Newton (1973). Its main feature is a high-pressure dome resulting in anticyclonic flow in the Canada Basin. The camps were initially placed near the center of the gyre and throughout the summer experienced a net southeastward drift,

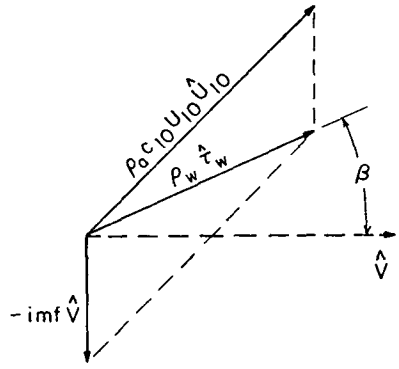

FIG. 6. Diagram of steady-state force balance. Carets indicate complex vectors. Variables without carets are scalar magnitudes.

gradually encountering increasing geostrophic flow. Currents were determined from the dynamic topography using a polynomial-fitting method developed for AIDJEX geostrophic wind analysis (M. Albright, personal communication).

There is some question whether the historical topography is appropriate because of anomalous drift patterns during 1975; nevertheless, in ice motion simulations, we found the sense, if not the magnitude, of the above geostrophic correction to be right. In all cases the magnitude was small (<3 cm s^{-1}). We shall show examples with and without the $\mathbf{V}_g$ correction to indicate its importance.

Given $\mathbf{V}$ and $\mathbf{U}_{10}$ we can proceed to solve (7) for $\boldsymbol{\tau}_w$ from each sample. Because of unavoidable uncertainties in prescribing the parameters for (7), our primary interest is in the shape of the stress versus velocity relationship rather than, say, deducing exact values for c_w. A straightforward statistical technique for such an investigation is to assume a relationship of the form $\tau_w = aV^b$ since the stress must vanish at $\mathbf{V} = 0$. We can then solve for the exponent b in a least-squares sense using linear regression analysis on the logarithmic equation $\log\tau_w = b \log V + \log a$. From the sample population we can estimate b and calculate an interval about the estimate within which we are confident to a given probability the actual value of b is contained.

In a discussion of the form expected for the stress-velocity curves in very simple models (McPhee, 1977b), we have shown that b ranges from unity in the case of the classical Ekman approach with constant eddy viscosity (of which slab models are a variant) to two for a case in which the eddy viscosity scaled by u_*^2/f is constant. The latter is clearly more closely related to the Businger-Arya model described here, but does not include the interaction of the surface layer which tends to increase the turning angle at low speeds (Fig. 5), thus increasing geostrophic drag. Therefore, we would expect a flow obeying the present model to have a

TABLE 1. Logarithmic regression slope estimates with 90% confidence limits for various combinations of c_{10}, m from all samples, $8 < V < 22$ cm s^{-1}. Numbers in parentheses are average values of β.

m (g cm^{-2})	c_{10} 0.0020	0.0025	0.0030
200	1.78 ± 0.12 (18.4°)	1.77 ± 0.12 (23.8°)	1.75 ± 0.12 (27.3°)
300	1.71 ± 0.11 (3.8°)	1.77 ± 0.12 (12.6°)	1.78 ± 0.12 (18.4°)
400	1.55 ± 0.09 (−10.4°)	1.69 ± 0.11 (0.9°)	1.75 ± 0.11 (8.7°)

logarithmic regression slope somewhat less than 2 but appreciably greater than 1.

Since (7) is a vector equation, each stress calculation also furnishes a value for β. However, note that β will be more sensitive to errors in c_{10}, m and V_g than the regression slope. This points up the problem alluded to earlier, namely, that a given uncertainty in the wind drag and ice mass will preclude determining the oceanic drag with any greater accuracy. Fortunately, there are certain helpful constraints in the problem. For instance, when allowance is made for the fact that manned ice station measurements are usually made over relatively smooth flows, results from the AIDJEX air stress program imply that c_{10} probably lies in the range 0.002–0.003 (E. Leavitt, personal communication). Similarly, probable brackets on the ice mass per unit area put m in the range 200–400 g cm^{-2}.

Table 1 shows the results of the regression analysis described above and the average value of β calculated from all samples in the range $8 < V < 22$ cm s^{-1} for various combinations of c_{10} and m. Error brackets on b indicate the 90% confidence interval, and we find that reasonable variation of c_{10} and m has only a minor effect on the *shape* of the stress-velocity curve. Note that none of the cases comes close to linear. As inspection of Fig. 6 implies, a twofold increase in ice mass can have a major effect on the average estimate for β. Since we expect

TABLE 2. As in Table 1 except no correction for V_g.

m (g cm^{-2})	c_{10} 0.0020	0.0025	0.0030
200	1.79 ± 0.14 (24.9°)	1.79 ± 0.13 (30.2°)	1.78 ± 0.13 (33.5°)
300	1.71 ± 0.13 (10.1°)	1.78 ± 0.14 (19.2°)	1.79 ± 0.14 (24.5°)
400	1.53 ± 0.11 (−4.8°)	1.67 ± 0.12 (7.1°)	1.75 ± 0.13 (15.2°)

TABLE 3. As in Table 1 except only samples $14 < V < 22$ cm s^{-1}.

m (g cm^{-2})	c_{10} 0.0020	0.0025	0.0030
200	1.75 ± 0.28 (22.7°)	1.75 ± 0.27 (26.9°)	1.74 ± 0.26 (29.5°)
300	1.68 ± 0.28 (11.1°)	1.73 ± 0.28 (18.2°)	1.75 ± 0.28 (22.7°)
400	1.54 ± 0.26 (−1.3°)	1.66 ± 0.28 (8.6°)	1.71 ± 0.28 (15.1°)

β to be of order 20–30° both from the 1972 data (McPhee and Smith, 1976) and from measurements of β_2 in the present work, we can use Table 1 to narrow the range of plausible c_{10}, m combinations. Table 2 is identical to Table 1 except that no correction for geostrophic current has been applied. Mean values of the regression slope are similar with slightly larger error brackets indicating more scatter in the stress estimates. Changes in β from Table 1 to Table 2 suggest the magnitude of errors associated with uncertainty in the geostrophic flow. One further test of the effect of uncertainties at lower speeds is presented in Table 3, where only samples in the range $14 < V < 22$ cm s^{-1} were considered. The reduced number of samples results in larger error brackets, but the regression slope estimates are not much changed. The increase in β for the higher speed population will be discussed in more detail in Section 4.

From these tables we can pick specific values for c_{10} and m for comparison with the model. By necessity the choice is somewhat arbitrary, but one can see that a tendency toward higher drag coefficients and lower mass is indicated by our calculations. From integrations of pilot balloon profiles at the AIDJEX sites, Leavitt (personal communication) inferred a value of 0.0027 for c_{10} at the central station. Using this, along with $m = 250$ g cm^{-2} (corresponding to mean ice thickness of ~2.7 m), stress was calculated according to (7) for each sample with speed in the range $8 < V < 22$ cm s^{-1}, and plotted in Fig. 7. The solid line is the least-squares curve from 254 samples, which is

$$\tau = 0.0104V^{(1.78\pm0.12)} \text{ [data]}. \quad (8)$$

The dashed line is the theoretical curve from Fig. 4 for $z_0 = 10$ cm. If one uses a similar least-squares analysis of the solutions used to produce the theoretical curve, the result is

$$\tau = 0.0131V^{(1.70\pm0.00)} \text{ [theory, } z_0 = 10 \text{ cm]}.$$

Thus, at the 90% confidence level, the logarithmic regression slope of the data points is not different from that of the model.

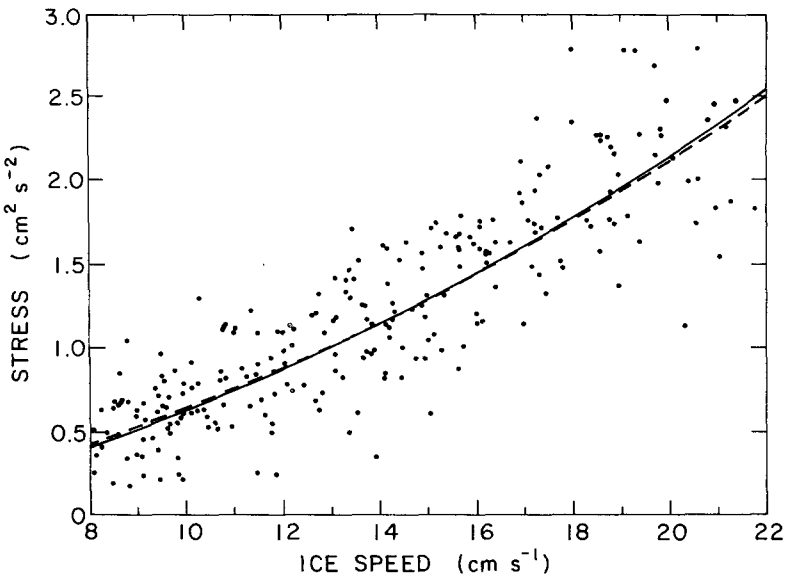

FIG. 7. Scatter diagram of stress estimates versus ice speed for $c_{10} = 0.0027$ and $m = 250$ g cm^{-2}. The solid line is best-fit exponential, $\tau = 0.0104V^{1.78}$; dashed curve is theoretical prediction with $z_0 = 10$ cm.

Fig. 8 shows β versus ice speed from the above calculations. The mean value for all samples was 20.4°, and the regression line is $\beta = (0.99 \pm 0.38)V + 6.74$. The slope is positive and different from zero at the 90% confidence level. It is clear from Tables 1–3 that the mean value of β is sensitive to a variety of factors and by itself is more a criterion by which a reasonable combination of m and c_{10} was chosen rather than a confirmation of the theory. It should be noted, however, that in all the plausible cases considered, the slope of regression of β against V is positive and different from zero at the 90% level of significance. This is counter to the theoretical trend shown in Fig. 5. Discussion of possible reasons for this behavior is deferred to the next section.

To this point, all observational comparison has come from surface wind and ice drift. We also had records from current meters suspended 2 m below the ice, which are important for two reasons.

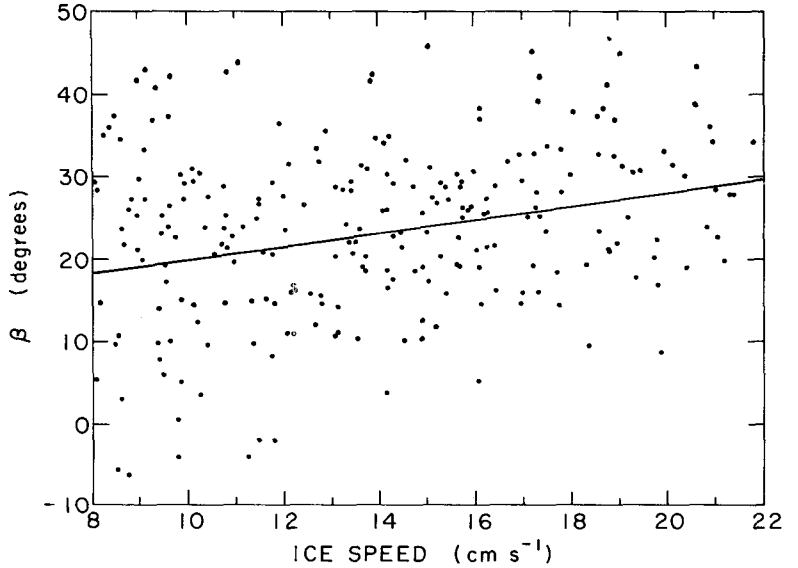

FIG. 8. Scatter diagram of β vs V for same parameters as Fig. 7. Solid line is least-squares straight line $\beta = 0.99V + 6.74$.

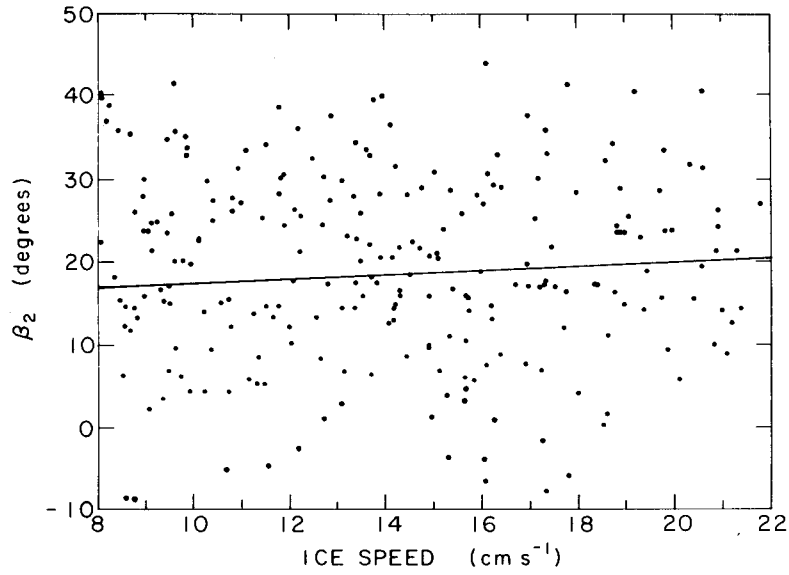

FIG. 9. β_2 vs V. The slope of the regression here is not significantly different from zero.

First, they furnish a measure of β_2, which is a fair approximation for β as Fig. 5 demonstrates, and second, they provide an independent check on the shape of the stress-velocity curve.

Fig. 9 shows values of β_2 as measured from all samples again in the range $8 < V < 22$ cm s^{-1}. The regression line drawn through the data shows no significant correlation between β_2 and V. Since errors in the current meter measurements, particularly in direction, were somewhat larger than anticipated (see McPhee, 1978b), the average value (18.4°) might be off by as much as ±5°. As with our estimates of β, there is large scatter in measurements of β_2: the standard deviation is 14.4° for β_2 compared with 14.7° for β. The correlation coefficient between β and β_2 is 0.30.

In order to estimate stress from the current at 2 m measured relative to the ice, it is necessary to assume a logarithmic current profile. For a typical stress of 1 cm^2 s^{-2}, 2 m corresponds to a nondimensional depth of approximately −0.03, which is within the range usually considered logarithmic (see, e.g., Tennekes, 1973). Using model calculations from Section 2, we found the predicted current at 2 m to deviate from logarithmic by less than 3% over the range of surface Rossby number considered; thus the approximation is theoretically quite good.

Given a logarithmic profile, the stress magnitude can be calculated as

$$\tau_2 = c_2 U_2^2, \tag{9}$$

where τ_2 is the *surface* stress, and

$$c_2 = \left[\frac{1}{k}\ln\left(\frac{200}{\bar{z}_{0L}}\right)\right]^{-2}. \tag{10}$$

Note that $\bar{z}_{0L}$ is a local surface roughness dependent on the chosen current meter sites and unlike the z_0 deduced above from model calculations, is not necessarily representative of the whole region.

What we seek is again the shape of the stress-velocity curve, this time using the stress obtained from a near-surface current meter, i.e.,

$$\tau_2 = a_2 V^{b_2}.$$

Taking logarithms and rearranging, we have

$$2\log U_2 = b_2 \log V + \log a_2 - \log c_2. \tag{11}$$

Note that c_2 and therefore $\bar{z}_{0L}$ do not affect the calculation of b_2. Table 4 shows least-squares solutions with 90% confidence intervals for b_2 from all camps (identified by their radio call-names) during the 60-day period. The value for Snowbird is appreciably different from the rest, and the fact that the size of the confidence interval is nearly triple the others suggests a possible malfunction of that speed sensor. Also shown are average values for β_2 from all camps. The value at Blue Fox is anomalously low, which might reflect either a consistent directional measurement error or perhaps the effect of local under-ice topography.

TABLE 4. Logarithmic regression slope estimates (b_2) and average departure angle ($\bar{\beta}_2$) by drift station, Days 201–261.

Camp	b_2	$\bar{\beta}_2$ (deg)
Big Bear	1.78 ± 0.25	21.4
Caribou	1.70 ± 0.36	25.6
Blue Fox	1.72 ± 0.37	8.2
Snowbird	2.54 ± 0.95	18.4

If data from Snowbird are disregarded, the combined samples imply

$$U_2^2 = 0.630V^{(1.71\pm0.18)}. \quad (12)$$

The logarithmic regression slope estimate is remarkably similar to both the theoretical and momentum balance estimates of b, and thus provides an independent confirmation of the theoretical approach.

The drag coefficient c_2 can be evaluated for the chosen values of c_{10} and m by combining (8), (9) and (12). Using an average value of $V = 14$ cm s^{-1}, the result is $c_2 = 0.020$. Having found c_2 we can use (11) to solve for a_2, with the expression for stress given approximately by

$$\tau_2 = 0.0126V^{1.71}.$$

The difference between this curve and the theoretical curve shown in Fig. 7 is barely perceptible.

The local surface roughness $\bar{z}_{0L}$ representing an average over three camps can be obtained from (10); with $c_2 = 0.020$, its value is $\bar{z}_{0L} = 11.7$ cm. A similar analysis treating momentum balance and U_2 data from each camp independently yielded the following values for $\bar{z}_{0L}$: Big Bear, 10.6 cm; Caribou, 13.1 cm; Blue Fox, 11.4 cm. Either the camps were very similar in both upper and lower surface characteristics (recall that a constant value of c_{10} was used), or if they were different, there was some compensating mechanism at work to keep, e.g., the ratio of upper and lower roughness approximately constant.

In spite of the fact that $\bar{z}_{0L}$ is quite similar to z_0 inferred from the model results, its large magnitude is puzzling. In the 1972 experiment (McPhee and Smith, 1976), we found the local surface roughness to be much smaller than what would be assumed representative of the surrounding region. This seemed reasonable since the camp was situated on a smooth floe and meant that the shear between the surface and 2 m was enhanced from what would be expected with a horizontally homogeneous surface. We found the ratio U_2/V to be about 0.85 in 1972 in contrast to a ratio of about 0.6 in 1975–76. The latter ratio remained fairly stable throughout the entire year (McPhee, 1978b, Table II). From upper surface indications the 1975–76 camps were similar to the 1972 camp. Adding to the mystery is work by Langleben (1977) who used a three-component ultrasonic current meter at station Caribou for a limited time in November 1975 to measure Reynolds stress and mean flow at 1 m. He inferred a roughness length of 1.9 mm. This is most likely a local "skin-friction" value and we would expect it to be much smaller than the model results, but by the same reasoning, we might expect U_2/V to be larger. Unfortunately, since Langleben (1977) does not relate the 1 m current to the ice velocity or 2 m current, the shape of the mean current profile is unknown. In summation, the 2 m current data confirm the theoretical shape of the stress-ice velocity curve (which should be independent of local surface characteristics) but also put us in the somewhat ironic position of not understanding why the measurements fit the theory so closely.

4. The effect of the pycnocline

It is well known that the turbulent exchange process can be strongly affected by buoyancy forces associated with fluid displacement in a stratified medium. Density of the water column in the central Arctic is controlled mainly by salinity and is usually characterized by a mixed layer 35–60 m deep over a strong halocline. In summer, melt water tends to stabilize the upper layer, so it is appropriate to ask what effect the density structure might have on statistics of ice drift and near-surface currents. The model of Section 2, which assumed uniform density in the water column, implied a dynamic boundary-layer depth proportional to u_*/f. The finite extent of the mixed layer imposes a third physical length scale z_{ML} on the problem which we expect to become increasingly important in PBL dynamics as the magnitude of the ratio fz_{ML}/u_* (which we shall call ξ_{ML}) becomes small; i.e., either as $|z_{ML}|$ decreases or surface stress increases. In this section we shall examine the effect of the pycnocline on the neutral model to form a qualitative impression of how it might change the surface drift statistics. Without a time-dependent treatment of inertial oscillations (such a study is underway), it is probably pointless to attempt much more.

It should be emphasized that the Businger-Arya (1974) model is more general than the neutral case considered heretofore, having been designed to investigate the stably stratified atmospheric PBL that occurs, e.g., when the surface undergoes rapid radiational cooling. While melting of sea ice during summer provides a negative buoyancy flux akin to those conditions, the rate of melting is usually too slow to cause a significantly stable surface layer unless the ice is nearly motionless. Nevertheless, we found in 1975 that the accumulated summer melting freshened the mixed layer and eventually established a secondary pycnocline at about 25–30 m, below which surface mixing rarely penetrated (McPhee, 1978b). In terms of modeling such behavior, we thought it more appropriate to consider a neutral layer bounded by a region in which the dimensionless eddy viscosity was reduced, rather than set up a negative buoyancy flux in the surface layer as Businger and Arya did. The simplest approach, then, was to let K_* vary as in the neutral model until it reached ξ_{ML}, below which it was assigned a smaller constant value. A proper model

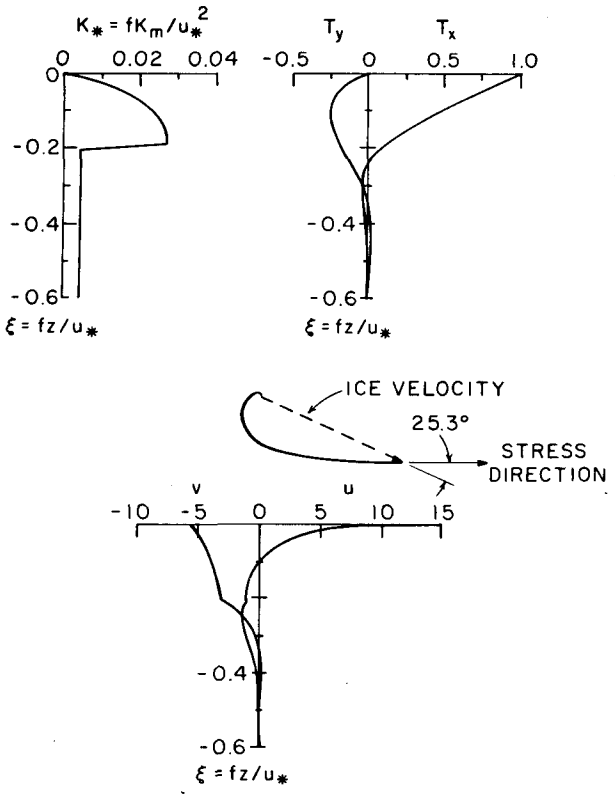

FIG. 10. PBL model results for $Ro_* = 1000$ except $K_* = 0.004$ for $|\xi| > 0.2$.

would probably express the K_* attenuation by some rational scheme like a local Richardson number dependence, but for the qualitative purposes here, we doubt the added complexity is warranted.

Fig. 10 shows results of a steady model in which K_* reduction occurs at $\xi_{ML} = -0.2$. If the mixed layer depth is $z_{ML} = -25$ m, this would correspond to a surface stress $u_*^2 = 3$ cm^2 s^{-2}, and is therefore a limiting case in the sense that $|\xi_{ML}|$ was rarely less than 0.2 at the AIDJEX camps when averaged over inertial cycles. Comparison with Fig. 1 shows that the surface characteristics have changed slightly—β is larger by about 2° and the drag has increased. A series of numerical experiments holding other parameters constant ($Ro_* = 1000$, $\xi_{ML} = -0.2$) shows how variations of K_* in the pycnocline affect surface characteristics and is summarized in Table 5. In general, the smaller K_* (corresponding to stronger stability), the more the turning and the greater the drag. The latter was unexpected, since stability in the atmosphere is generally associated with a decrease in geostrophic drag. A few model experiments demonstrated, however, that the drag decreased only if K_* was decreased at a level above the one where it otherwise reached its maximum value (which, incidentally, seemed to coincide under maximum stress conditions with the summer mixed-layer depth). Since ξ_{ML} was nearly always deeper than the K_* maximum, this theoretically has an interesting consequence, i.e., for a given ice velocity and mixed-layer depth, the surface stress would increase with increasing stability of the pycnocline. The effect would be more pronounced at higher speeds because ξ_{ML} would be nearer the K_* maximum. In terms of the stress-velocity curve, the effect would be to increase b from its neutral value.

There is some evidence that behavior similar to that described above in fact occurred. First, there is the apparent increase in β with speed mentioned in the previous section. Unfortunately, the scatter in the data is large, the calculation is sensitive to a number of assumptions, and there was no statistically significant correlation between β_2 and ice speed; thus, the β argument by itself is hardly compelling. A second factor, however, is demonstrated by Fig. 11, which shows least-squares exponential curves of τ vs V calculated by the stress-balance method for three 20-day blocks spanning the original "free drift" period (days 201–261). Note that the middle period (labeled 2) beginning 9 August 1975 (day 221) shows higher stress at higher speeds, which means in the parlance of the last section that b is greater. Calculated values for b with 90% confidence limits are as follows:

$$201\text{–}221: \quad b = 1.62 \pm 0.14$$

$$221\text{–}241: \quad b = 2.04 \pm 0.19$$

$$241\text{–}261: \quad b = 1.66 \pm 0.26.$$

The first and second periods are significantly different from each other, only the second period is different from the neutral model.

As Fig. 12 shows, the mixed-layer depth remained roughly constant over the entire period, but its salinity gradually decreased throughout August until surface freezing reversed the trend about day 240. We would thus expect a sharper density interface (smaller K_* in the pycnocline) during the middle period, and according to our simplified "high inversion" model, more drag at higher speeds. This is consistent with the data.

Although the mean ice speed was similar in all three periods, the level of inertial motion was

TABLE 5. Surface drag coefficient and departure angle for various values of K_* in pycnoline. $Ro_* = 1000$ and $|\xi| = 0.2$ in all cases. Decreasing K_* implies increasing stability.

	K_* (pycnocline)				
	(Neutral)	0.010	0.004	0.002	0.001
C_w ($\times 10^3$)	5.4	5.6	5.9	6.0	6.2
β (deg)	23.1	24.5	25.3	25.7	26.1

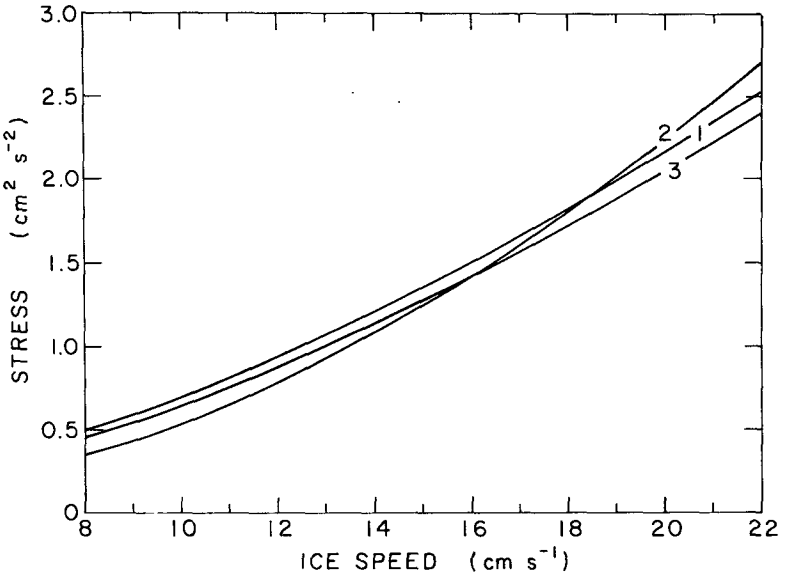

FIG. 11. Least-square-fit exponential stress-velocity curves for each of three 20-day periods: 1, Days 201–221; 2, Days 221–241; 3, Days 241–261. Note that curve 2 indicates higher drag at higher speeds.

highest during the second period, suggesting that the pycnocline effect would be more pronounced then. It seems clear that once the pycnocline becomes important in the problem, the steady-state assumption for mean properties of the PBL becomes less valid: one can visualize the dynamic PBL depth oscillating up and down in response to surface inertial motions (McPhee, 1978a) and being "clipped" when it reaches the density interface. Such behavior would be intrinsically nonlinear.

There are many questions raised in this section that call for discussion in greater depth, but which are probably beyond the scope of both the simple model and the limited measurements described. Our main purpose has been to demonstrate that mean surface characteristics are not greatly affected by the presence of a pycnocline, unless it happens to be quite shallow.

5. Conclusions

We have shown that the mean properties of surface velocity and stress as inferred both from surface drift measurements (modified by the Coriolis force in the ice) and from near-surface current measurements are consistent with a simple steady-state PBL model, even when significant inertial period motion is present. The important principles are that the physical parameters (including eddy viscosity) be scaled by u_*, u_*^2 and u_*/f for velocity, kinematic stress and length; and that the nondimensional eddy viscosity fall off linearly near the ice-ocean interface in order to allow a logarithmic surface layer. Within this general framework, details of the K_* distribution are probably not overly important, but we consider the scheme advanced by Businger and Arya (1974) to be attractive because it obviates, for example, the need to arbitrarily specify a maximum value for K_*.

While details of the surface layer in the open ocean must be quite different from that under ice, it seems plausible that below a few meters, one might expect to see a current structure averaged over inertial cycles quite similar to that measured under pack ice

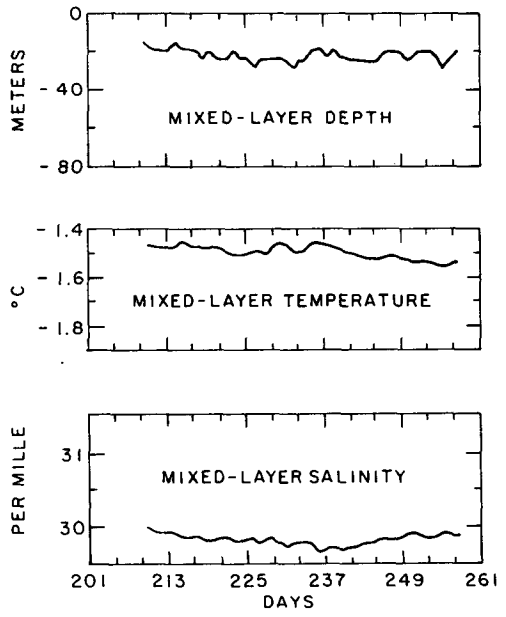

FIG. 12. Mixed-layer chracteristics at station Snowbird, Days 201–261, adapted from McPhee (1978b).

(McPhee and Smith, 1976). As we mentioned before, if the primary interest is what happens at the density interface, a time-dependent model may be needed; nevertheless, the fundamental concept that the turbulent structure is constantly scaling itself to surface conditions gains considerable credence from these results.

If the interest is surface velocity, as it often is for ice modeling, we seek a relationship of the form

$$\mathbf{V} = c_\tau \mathbf{u}_* e^{-i\beta}, \tag{13}$$

where $\mathbf{u}_* = \boldsymbol{\tau}_s/\sqrt{\tau_s}$ and c_τ and β are in general functions of Ro_* (i.e., f, z_0, u_*). In previous drift calculations and in the AIDJEX pack ice model, we have set c_τ and β constant resulting in a quadratic stress-velocity relationship ($b = 2$). With Rossby-number similarity theory (Blackadar and Tennekes, 1968) we can generalize (13) but retain reasonably simple expressions for c_τ and β. The theory is that at high enough Rossby number, the effect of the surface is felt only in the u component very near the surface. Beyond this thin layer, all velocity profiles will be similar if scaled properly; it is essentially the argument made in Section 2 regarding extrapolation of the present results to the open ocean, where knowledge of z_0 is scarce. Stated simply, requirements of the theory for the nondimensional velocity components are

$$v = \text{constant} = -B/k,$$

$$u = k^{-1}(\ln \mathrm{Ro}_* - A).$$

Thus,

$$\beta = \tan^{-1}[-B/(\ln \mathrm{Ro}_* - A)], \tag{14}$$

$$c_\tau = k^{-1}[B^2 + (\ln \mathrm{Ro}_* - A)^2]^{1/2}. \tag{15}$$

Curves of τ and β vs V calculated using (14) and (15) with $z_0 = 10$ cm, $A = 1.91$ and $B = 2.12$ are shown in Figs. 4 and 5. In the model, A and B themselves depend weakly on Ro_* (especially at low values of Ro_*) as the slight discrepancy in β indicates. However, the added complexity of deriving different functional forms for c_τ and β from the model is hardly justified in light of other uncertainties.

Finally, we wish to reiterate that while quantitative details (numerical values of z_0, A, B, etc.) of this work depend on specification of surface wind stress and ice mass and will therefore reflect fairly large uncertainties, the general behavior of surface stress and velocity is quite well described by the simple model. The work thus underscores the premise that pack ice provides an excellent laboratory for boundary layer experimentation appropriate to both the atmosphere and the open ocean.

Acknowledgments. The author is indebted to the AIDJEX staff for help with data processing and organization. L. Timokhov and I. Kulakov kindly furnished the PBL solution technique. This work was supported by the National Science Foundation under Grant DPP 77 17341 and by AIDJEX.

REFERENCES

Blackadar, A. K., and H. Tennekes, 1968. Asymptotic similarity in neutral planetary boundary layers. *J. Atmos. Sci.*, **25**, 1015–1019.

Businger, J. A., and S. P. S. Arya, 1974. The height of the mixed layer in a stably stratified planetary boundary layer. *Advances in Geophysics*, Vol. 18A, Academic Press, 73–92.

Deardorff, J. W., 1972. Numerical investigation of neutral and unstable planetary boundary layers. *J. Atmos. Sci.*, **29**, 91–115.

Langleben, M. P., 1977. Water drag coefficient at AIDJEX, station Caribou. Paper presented at A Symposium on Sea Ice Processes and Models, Seattle, Washington, September 6–9, 1977. Proceedings to be published by University of Washington Press.

McPhee, M. G., 1977a. An analysis of pack ice drift in summer. Paper presented at A Symposium on Sea Ice Process and Models, Seattle, Washington, September 6–9, 1977. Proceedings to be published by University of Washington Press.

——, 1977b. Unpublished manuscript. On boundary-layer scaling and the drift of pack ice. *Ocean Modelling*, No. 7 (August).

——, 1978a. A simulation of inertial oscillation in drifting pack ice. *Dyn. Atmos. Oceans*, **2**, 107–122.

——, 1978b. AIDJEX Oceanographic Data Report. *AIDJEX Bull.*, No. 39 (May), 33–78.

McPhee, M. G., and J. D. Smith, 1976. Measurements of the turbulent boundary layer under pack ice. *J. Phys. Oceanogr.*, **6**, 696–711.

Newton, J. L., 1973. The Canada Basin; mean circulation and intermediate scale flow features. Ph.D. thesis, University of Washington, Seattle, 158 pp.

Stern, M. E., 1975. *Ocean Circulation Physics*. Academic Press, 246 pp.

Tennekes, H., 1973. The logarithmic wind profile. *J. Atmos. Sci.*, **30**, 234–239.

Timokhov, L., R. Brown, I. Kulakov, E. Leavitt, G. Trushina, and R. Colony, 1976. A description of a model of the atmospheric boundary layer. *AIDJEX Bull.*, No. 33 (September), 95–101.

Wyngaard, J. C., O. R. Coté and K. S. Rao, 1974. Modeling the atmospheric boundary layer. *Advances in Geophysics*, Vol. 18A, Academic Press, 193–212.